Full Paper

Propellants, Explosives, Pyrotechnics

DOI: 10.1002/prep.201800104

A Systematic Method to Determine and Test the Ignition and Growth Reactive Flow Model Parameters of a Newly Designed Polymer-Bonded Explosive

Xiao Li,[a] Yi Sun,*[a] Hongda Zhao,[a] Youcai Xiao,[b] Xuanming Cai,[c] Qiuhua Zhang,[a] and Wei Zhang[a]

Abstract: In this paper, a systematic method to determine and test the ignition and growth reactive flow model parameters of a new energetic material PBX 1314 (60 weight% RDX, 16 weight% aluminum and 24 weight% HTPB) is presented. Cylinder test and shock initiation experiments are performed to study the shock initiation property of the explosive. Ignition and growth parameters are determined based on the experimental data. Test of the obtained parameters is performed by the comparison of the reaction fraction in the impact initiation and energy release experiments and the corresponding numerical simulations. The simulation results reveal that the proceeding of reaction and energy release are unsteady and inhomogeneous. Pressure decline quenches the reaction in the impact layer of the specimen although the impact pressure is more than 7 GPa. Wave reflection and superposition strengthen the pressure in the top of the specimen and triggers detonation.

Keywords: Ignition and growth reactive flow model · Polymer-bonded explosives · Cylinder test · Shock initiation experiment · Unsteady reaction

1 Introduction

Heterogeneous polymer-bonded explosives consist of energetic crystalline grains, inert viscoelastic polymer binder and other additives. Reaction and energy release occur when the explosives encounter impact, friction, or shock wave with adequate strength. It is commonly accepted that the formation of hot spots results in the initiation. Several of mechanisms such as localized adiabatic shear, void collapse, interface friction and viscous heating in the energetic material lead to the formation of the hot spots [1,2]. Theoretical models are developed to describe the shock initiation and energy release process quantitatively. The first category [3,4] treats the heterogeneous material as a homogeneous mixture of the reactants and reaction products during the reaction. A single variable is introduced to represent the reaction quantitatively. The second group [5–8] treats the solid reactants and gas products separately. They consist of the balance laws of mass, momentum, energy for each phase, and the equations that allow solid phase compression. The third group [9–11] studies the hot spots formation mechanisms in microstructural level by the implementation of the cohesive finite element method.

The ignition and growth reactive flow model, which belongs to the first category of theoretical models, is widely used in characterizing the shock initiation property of energetic materials. It was presented [3] and improved [12] to describe different reaction process in shock initiation. The ignition and growth reactive flow model parameters of different kinds of energetic materials have been determined by the shock initiation experiments [13–15]. Tests of the obtained parameters were carried out by the particle velocity histories in Sideways Plate Push Tests [16], the breakout time in hockey puck experiments [17] and the critical gap thicknesses or critical projectile impact velocities in gap tests [14]. However, the variables in experiments were not explicit in the ignition and growth reactive flow model. Direct verifications based on an explicit variable such as the reaction fraction are rarely reported.

Investigations on the reaction efficiency of the energetic material have been done in previous researches. The vent tests [18] were designed and modified [19–22] to study the impact-initiated chemical reaction characters of reactive materials. Temperature controlled thermochemical models were proposed [20,21] to calculate the extent of reaction of the multifunctional energetic structural materials. Reaction efficiencies of the polymer-bonded explosive specimens in

[a] *X. Li, Y. Sun, H. Zhao, Q. Zhang, W. Zhang*
Department of Astronautic Science and Mechanics
Harbin Institute of Technology
Harbin 150001, P. R. China
**e-mail: sunyi@hit.edu.cn*
[b] *Y. Xiao*
College of Mechatronic Engineering
North University of China
Taiyuan 030051, P. R. China
[c] *X. Cai*
School of Science
North University of China
Taiyuan 030051, P. R. China

impact initiation and energy release experiments were obtained based on the assumption that the increment of the released energy into the chamber is proportional to that of the reaction efficiencies of the specimens [22]. The experiment results [22] make the verification of the ignition and growth reactive flow model parameters attainable. The inhomogeneity of the reaction in the specimen could also be analyzed for the convenience of the numerical simulation.

In this paper, a systematic method to determine and verify the ignition and growth reactive flow parameters of a new designed polymer-bonded explosive PBX 1314 (60 weight% RDX, 16 weight% aluminum and 24 weight% HTPB) is presented. As for the PBX1314, the dynamic mechanical behavior and damage character have been previously investigated [23, 24]. In this work, the shock initiation property of PBX 1314 is studied by the conduct of cylinder test and shock initiation experiments. The ignition and growth reactive flow model parameters are determined on the basis of the experimental results. Tests of the obtained parameters are performed by numerical simulations of the reaction of the PBX1314 specimens in the impact initiation and energy release experiments. Details of the reaction process of the specimens are analyzed based on the numerical simulation results. The effect of the impact loads and boundary conditions on the reaction process of the specimens are investigated. Instability and non-uniformity of the reaction in different regions of the specimens are considered.

2 Experimental Section

2.1 Cylinder Test

The experimental configuration is shown schematically in Figure 1. A copper tube of 50 mm inner diameter and 495 mm long is filled with PBX1314. Two PBX 1314 cylinder specimens of 50 mm diameter and 50 mm thick are stacked at both ends of the tube. The left specimen is initiated by the detonator in the beginning. Steady detonation waves form in the left specimen and propagates to the one in the copper tube and finally to the one on the right. The steady detonation velocity comes from the two electric pins embedded in the two terminals of the specimen in the copper tube. A back-light system and a high speed camera are used to record the radial displacement of the copper tube in the cross section of 200 mm away from the right terminal. The expansion history of the copper tube is used to determine the equation of state of the PBX 1314 detonation products.

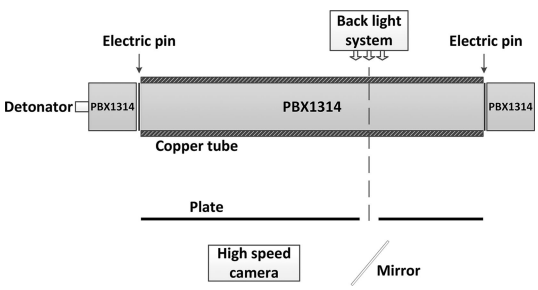

Figure 1. Schematic diagram of the cylinder test of PBX 1314.

2.2 Shock Initiation Experiment

A photograph of a typical shock initiation experiment composed of disks of PBX 1314, Teflon encapsulated manganin gauges, and aluminum plates is shown in Figure 2. In this work, PBX 1314 is cast into short cylinder specimens ranging from 2 to 25 mm in height and 50 mm in diameter. Various thicknesses of the cylinder specimens are used to measure the pressure histories at various distances into PBX1314. Embedded manganin pressure gauges are placed along the axes of the specimens, which are initiated by the donor explosive. We varied the input pressure to the specimens by changing the thickness of the aluminum plates. The active manganin elements are 0.025 mm thick and are encapsulated in Teflon, which is an excellent impedance match for these specimens. During the experiments, the manganin gauge voltage traces are recorded by an oscilloscope and converted to pressure traces over time by using the pressure-piezoresistance relationships.

Figure 2. Photograph of a typical shock initiation experiment.

3 Results and Discussion

3.1 Equation of State Parameters of Reactants and Detonation Products

The ignition and growth reactive flow model has been widely used for its good performance in characterizing the shock initiation process of energetic materials. In this model, the Jones-Wilkins-Lee (JWL) equations of state of the unreacted explosive and the reaction products are both in temperature dependent form

$$p_e = A_e e^{-R_{1e}V_e} + B_e e^{-R_{2e}V_e} + \omega_e C_{Ve} T_e / V_e \quad (1)$$

$$p_g = A_g e^{-R_{1g}V_g} + B_g e^{-R_{2g}V_g} + \omega_g C_{Vg} T_g / V_g \quad (2)$$

in which p is pressure, V is relative volume, ω is the Gruneisen coefficient, C_V is average heat capacity, T is temperature, and A, B, R_1, R_2 are constants. The subscript e and g denote the unreacted explosive and the reaction products, respectively. The mixture rule assumes the unreacted explosive and the reaction products have the same pressure and temperature. The reaction rate law is expressed as

$$df/dt = I(1-f)^b(\rho/\rho_0 - 1 - a)^x + G_1(1-f)^c f^d p^y + G_2(1-f)^e f^g p^z \quad (3)$$

where f is the reaction fraction of the explosive, ρ is the current density, ρ_0 is the initial density, a is the compression limit, and b, c, d, e, g, x, y, z, I, G_1 and G_2 are constants.

The JWL equation of state of the unreacted explosive is determined by the Hugoniot data obtained from flyer plate impact experiments [25]. The fitting parameters are listed in Table 1.

Table 1. JWL parameters of the reactants.

Parameter	A(GPa)	B(GPa)	R_1	R_2	ω	Cv (GPa K^{-1})
Value	83160	−8.0	11.85	1.895	0.894	2.487×10^{-3}

The reaction product JWL equation of state is calculated by using the methods described by Lan [26] and Souers [27]. The time dependence of the radial displacement and velocity of the tube are expressed as

$$r_m - r_{m0} = \sum_{j=1}^{2} a_{mj}\left[t - \left(1 - e^{-b_{mj}t}\right)e^{-b_{mj}t_{m0}}/b_{mj}\right] \quad (4)$$

$$dr_m/dt = \sum_{j=1}^{2} a_j\left(1 - e^{-b_j t_i}\right) \quad (5)$$

in which r_{m0} and r_m denote radius of central surfaces of the tube for the initial and a given moment, respectively. a_{mj}, b_{mj}, t_{m0} are parameters. The acceleration of the central surface is acquired by transforming the data in Eulerian coordinate to that in Lagrangian coordinate. The p–V relation is obtained from equations of conservation laws. JWL parameters are then calculated by nonlinear fitting codes. Figure 3 shows the expansion history of the copper tube in cylinder test in subsection 2.1. The calculated JWL parameters of PBX 1314 reaction product based on the experimental data

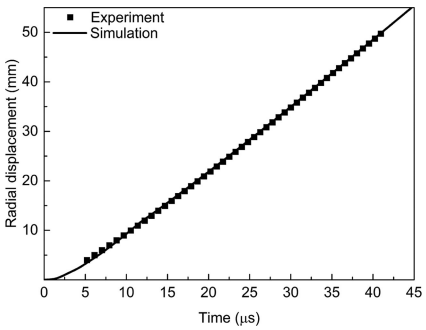

Figure 3. Radial expansion histories of the scanned cross section of the copper tube in cylinder test and numerical simulation.

in Figure 3 are listed in Table 2. Numerical simulation of the steady detonation wave propagation and the copper tube expansion in the cylinder test is performed. The simulated radial displacement of the copper tube is in good agreement with the experimental data. The A and B in Table 2, which are the coefficients of the two terms corresponding to the high and medium pressure state, are both less than those of another aluminized explosive PBXN-109 (64 weight % RDX, 20 weight % Aluminium and 16 weight % binder) [28]. It is due to the less weight percentage of RDX and aluminium in PBX 1314.

3.2 Ignition and Growth Reactive Flow Model Parameters of PBX 1314

The embedded gauge records in the shock initiation experiments are shown in Figure 4. These traces exhibit the feature of shock initiation of heterogeneous explosives: some reaction occurs just behind the shock front causing it to grow in pressure, but most of the reaction occurs well behind the leading shock. The latter reaction creates a pressure wave that overtakes the initial shock and causes transition to detonation. The decrease of pressure at the 0 mm gauge positions are attributed to the endothermic process before the rapid exothermic reaction begins. In this process, aluminium acts as a diluent or even as an endothermic component and reduces the pressure.

Parameters of the ignition and growth reactive flow model in Table 3 are obtained by the pressure histories in the shock initiation experiments and the Lagrange analysis method [29]. Parameters in Table 1, 2 and 3 are implemented into finite element models to simulate the shock initiation process of PBX 1314. The good agreement between the calculated pressure traces and the experimental

Table 2. JWL parameters of the reaction products.

Parameter	A(GPa)	B(GPa)	R_1	R_2	ω	Cv (GPa K^{-1})
Value	763.1	1.474	4.483	0.497	0.316	1.00×10^{-3}

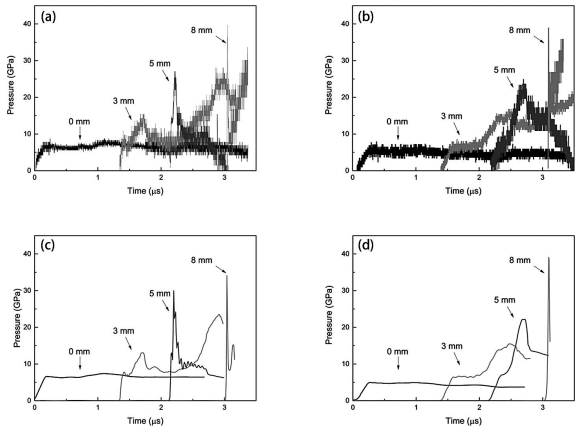

Figure 4. Pressure histories in four different Lagrange depths in shock initiation experiments and numerical simulations: (a) Pressure histories in the first experiment, (b) Pressure histories in the second experiment, (c) Simulated pressure histories correspond to the first experiment, (d) Simulated pressure histories correspond to the second experiment.

Table 3. Ignition and growth model parameters.

Parameter	Value	Parameter	Value
I (μs^{-1})	8×10^4	G_2 ($GPa^{-2}\mu s^{-1}$)	0.0073
a	0.100	e	0.300
b	0.667	g	0.333
x	7	z	2
G_1 ($GPa^{-2}\mu s^{-1}$)	0.006	F_{igmax}	0.5
c	0.667	F_{G1max}	0.5
d	0.333	F_{G2min}	0.08
y	2	–	–

results in Figure 4 indicates the accuracy of the obtained parameters in Table 3.

It is worth noting that the parameter G_1 in Table 3, which plays a dominant role in determining the growth of reaction, is smaller than that of PBXN-109 [28]. The difference is due to the less content of aluminium in PBX 1314. In the reaction growth stage, the less aluminium provides smaller burning surface area and the neighbouring explosive particles are consumed at lower rates. Therefore the reaction and the energy release proceed in lower rates.

3.3 Verification of the Model Parameters of PBX 1314

In the impact initiation and energy release experiments [22], the explosive specimens are launched by a gun barrel and impact an anvil in a quasi-sealed chamber. The impact initiates the specimens and gas products are released into the quasi-sealed space. The increased gas pressure in the space is measured to quantify the released energy from the reacted specimens according to the relationship [18]

$$\Delta P = \Delta E\left(\gamma - 1\right)/V \tag{6}$$

where γ is the ratio of specific heats of the gas, V is the volume of the test chamber, ΔP and ΔE are the gas pressure and released energy into the gas in the chamber, respectively. Reaction efficiency of the specimen, η, is defined as

$$\eta = \Delta E/\Delta E_{\max} = \Delta P/\Delta P_{\max} \tag{7}$$

in which ΔE_{max} and ΔP_{max} refer to maximum of ΔE and ΔP. Based on Equation (6) and (7), the reaction efficiencies of the specimens at different impact velocities are determined. It should be noted that the reaction efficiency equals to the reaction fraction f in the ignition and growth reactive flow model. Therefore the impact initiation and energy release experiments provide credible data to test the ignition and growth reactive flow model parameters of PBX 1314.

Numerical simulations of the initiation process of PBX 1314 in the impact initiation and energy release experiments are conducted in this work. The finite element model is shown in Figure 5. In consideration of the 0.5 mm thickness of the aluminium seal-plate, the loss of projectile velocity and specimen mass during penetration are ignored reasonably. Only the impact between the projectiles embedded with cylinder energetic material specimens and the anvil are considered. To simplify the calculation, only a quarter of the projectile, specimen and anvil are simulated. Boundary constraints are added to the symmetric plane and the back of the anvil.

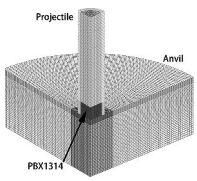

Figure 5. Finite element model of the confined PBX 1314 specimen and anvil in impact initiation and energy release experiment.

The simulated reaction efficiencies of the specimens at different impact velocities are plotted in Figure 6 along with the experimental results. In general, the simulated reaction efficiencies of the specimens produced good agreement with the experiment results. The reaction efficiencies are both zero at 200 m/s and 250 m/s in simulation results, which indicate the specimens are only compressed mechanically and no chemical reaction occurs. When impact velocity increases to 300 m/s, the maximum reaction efficiency turns to 0.07, which reveals that only a small amount

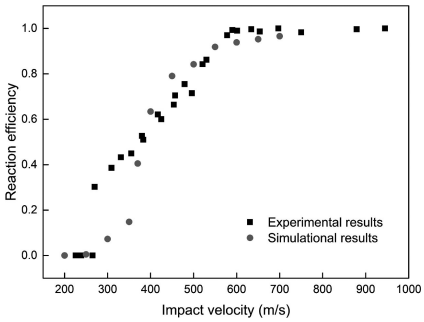

Figure 6. Comparison of reaction fraction at different impact velocities in experiments and numerical simulations.

of the specimen is initiated and the reaction quenches immediately. As impact velocity increases from 350 m/s to 400 m/s, the reaction efficiency ascends steeply from 0.15 to 0.41. This steep rise of reaction efficiency reveals that the fast reaction term of the ignition and growth reactive flow model is activated in more region of the specimen and more material is consumed.

As the impact velocity goes on increasing, the enhanced input pressure to the specimen further intensifies the reaction. The reaction efficiency continues rising and reaches its maximum 1.0 at 700 m/s. It means the velocity of 700 m/s is sufficient to cause the complete reaction of the specimen. Reexamination of the experiment results reveals that the maximum gas pressure is 0.298 MPa in Shot No. 23 rather than 0.296 MPa in Shot No. 19. The second impact velocity threshold should be 697 m/s instead of 590 m/s. Consequently, the calculated threshold 700 m/s is only 0.4% larger than the experimental result.

The analysis on Figure 6 illustrates that the finite element model in this work accurately calculated the reaction fractions of the specimens in the impact initiation and energy release experiments. The accuracy indicates that the parameters of the ignition and growth reactive flow model determined from the systematic work in subsection 3.1 and 3.2 could well characterize the initiation and energy release process of the specimens under complex loading.

3.4 Instability and Non-Uniformity of the Reaction of the Specimen

As the ignition and growth reactive flow model parameters have been verified, it is convenient to analyze the reaction and energy release process in detail by numerical simulation. The simulation result at 400 m/s in subsection 3.3 is taken for instance to investigate the reaction evolution and energy release in the specimen. In consideration of the axial symmetry, the pressure and reaction fraction fields in the specimen at different moments are plotted from the view of the XOY symmetry plane in Figure 7 and Figure 8. The symmetry axes of the specimens are represented by dashed lines. The move direction of the specimens are denoted by arrows. The solid lines close to the bottom of the specimens refer to the impact planes between the specimens and the anvils. The pressure and reaction efficiency histories of four representative elements are shown in Figure 9.

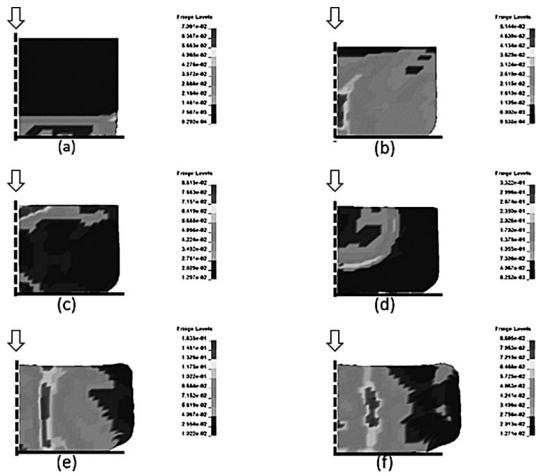

Figure 7. Pressure of the specimen at different moments, (a) $t=$ 0.24430 μs, (b) $t=1.36678$ μs, (c) $t=1.63333$ μs, (d) $t=2.07504$ μs, (e) $t=3.14647$ μs, (f) $t=3.62402$ μs. The arrows denote the move direction of the charges. The black solid lines below the charges denote the anvil on which the charges impact. The dashed lines represent the symmetry axis of the specimens.

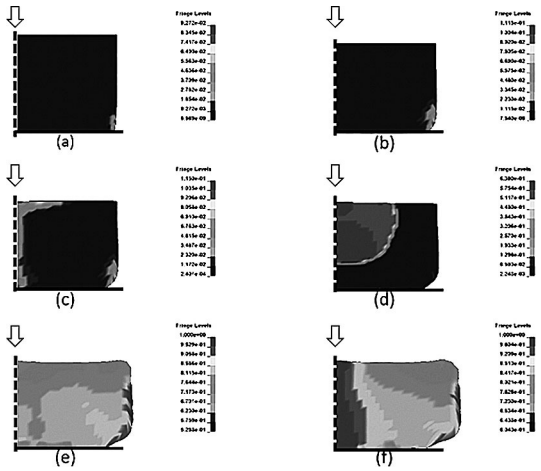

Figure 8. Reaction efficiency of the specimen at different moments, (a) $t=0.24430$ μs, (b) $t=1.36678$ μs, (c) $t=1.63333$ μs, (d) $t=$ 2.07504 μs, (e) $t=3.14647$ μs, (f) $t=3.62402$ μs. The arrows denote the move direction of the charges. The black solid lines below the charges denote the anvil on which the charges impact. The dashed lines represent the symmetry axis of the specimens.

Initially, the impact between the specimen and the anvil produces plane stress waves in the specimen. This corresponds to the first peaks of pressure in Figure 9 (a) and (b). Material in the bottom is compressed and temperature increases after the wave front. Accumulation of heats leads to

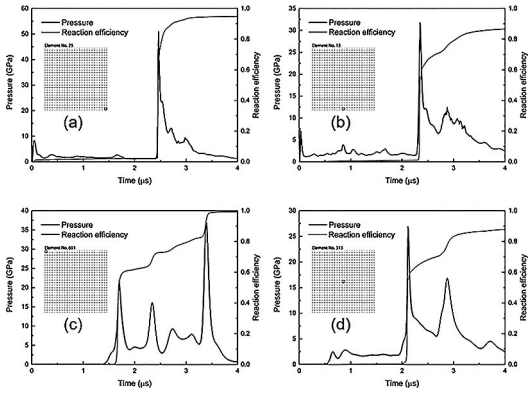

Figure 9. Pressure and reaction efficiency history of four different element in PBX1314 specimen, (a) Element No. 25, (b) Element No. 13, (c) Element No. 601, (d) Element No. 313.

the formation of hot spots and ignition. However, the ductility of copper causes deformation of the projectile head after the initial impact. The small diameter of the specimen results in a large ratio of the lateral area to the volume. The expanding deformation absorbs energy and decreases the pressure of bottom of the specimen by 75 %. The hot spots stop burning and the reaction rate decreases to zero. This is very different from the circumstance in the shock initiation experiments. It indicates the lateral confine also plays a significant role in the unsteady evolution of the reaction.

The weakened input stress waves propagate upward. Meanwhile, the reflected waves generated on the interface of the specimen and the projectile due to impedance difference propagate inward. The reaction during this process is weak and the reaction fraction is less than 0.05. The reflected waves superpose at the axis in Figure 7 (b) and then reaches the top centre where the material is ignited. The reaction fraction exceeds F_{G2min} so the third term of the ignition and growth reactive flow model is activated. The reaction rate exceeds $10^7\ \mu s^{-1}$. It results in the steep rise of both reaction efficiency and pressure at the moment of 1.7 μs in Figure 9 (c). The detonation waves then move outward and ignite the material in other regions. Pressure and reaction efficiencies of the elements in different regions of the specimen are abruptly enhanced in sequence. This process is illustrated in Figure 8 (d). In the following, reflection and superposition of stress waves carry the reaction forward, and finally 62 % of the specimen is consumed.

The analysis of Figure 7, 8 and 9 reveals that the reaction is unsteady in each region of the specimen and uneven among different parts of the specimen. This is attributed to not only the effect of confine and wave superposition but also the role of pressure and temperature in the reaction process. The deformation of the projectile head causes pressure decrease in some regions of the specimen. The reaction is weakened and releases little energy to the region behind the wave front. As the projectile continues expanding, the reaction is stopped. In contrast, the wave superposition generates higher pressure and temperature in other regions of the specimen. It leads to the faster rates of reaction and energy release in these regions. Pressure and temperature increase in return. The waves strengthened by the increased pressure go to the neighbouring region where the reaction is accelerated in the following stage.

4 Conclusions

A systematic method to determine and test the ignition and growth reactive flow model parameters of a newly designed energetic material PBX 1314 is presented in this work. The cylinder test and shock initiation experiments are performed to understand the shock initiation property of PBX 1314. Determination of the parameters of ignition and growth reactive flow model of the explosive is conducted based on the experiment data. Agreement between experiments and the corresponding numerical simulations is achieved by use of the obtained parameters. Test of the ignition and growth reactive flow model parameters is performed by the numerical simulation of the reaction process of the specimens in the impact initiation and energy release experiments. The pressure and reaction efficiency fields calculated by the ignition and growth reactive flow model reveal that the reaction in the specimen is unsteady and non-uniform. This is due to the non-stable and uneven pressure field in the specimen. The non-stable and uneven feature of the pressure field is generated by the deformation of the projectile and wave superposition.

Acknowledgements

The presented work was supported by the Aerospace Science and Technology Innovation Fund Projects of Harbin Institute of Technology [grant numbers CASA-HIT12-1 A02].

References

[1] J. E. Field, Hot spot ignition mechanisms for explosives, *Acc. Chem. Res.* **1992**, *25*, 489–496.
[2] Y.-Q. Wu, F.-L. Huang, Experimental Investigations on a Layer of HMX Explosive Crystals in Response to Drop-Weight Impact, *Combust. Sci. Technol.* **2013**, *185*, 269–292.
[3] E. L. Lee, C. M. Tarver, Phenomenological model of shock initiation in heterogeneous explosives, *Phys. Fluids* **1980**, *23*, 2362–2372.
[4] J. N. Johnson, P. K. Tang, C. A. Forest, Shock-wave initiation of heterogeneous reactive solids, *J. Appl. Phys.* **1985**, *57*, 4323–4334.
[5] B. P. B. Kang J, Baer M R, A thermomechanical analysis of hot spot formation in condensed-phase, energetic materials, *Combust. Flame* **1992**, *89*, 117–139.

[6] J. Massoni, R. Saurel, G. Baudin, G. Demol, A mechanistic model for shock initiation of solid explosives, *Phys. Fluids* **1999**, *11*, 710–736.
[7] D. A. LaBarbera, M. A. Zikry, The effects of microstructural defects on hot spot formation in cyclotrimethylenetrinitramine-polychlorotrifluoroethylene energetic aggregates, *J. Appl. Phys.* **2013**, *113*, 243502-14.
[8] M. Akiki, S. Menon, A model for hot spot formation in shocked energetic materials, *Combust. Flame* **2015**, *162*, 1759–1771.
[9] A. Barua, M. Zhou, A Lagrangian framework for analyzing microstructural level response of polymer-bonded explosives, *Modell. Simul. Mater. Sci. Eng.* **2011**, *19*, 055001.
[10] A. Barua, Y. Horie, M. Zhou, Energy localization in HMX-Estane polymer-bonded explosives during impact loading, *J. Appl. Phys.* **2012**, *111*, 399–586.
[11] A. Barua, S. Kim, Y. Horie, M. Zhou, Ignition criterion for heterogeneous energetic materials based on hotspot size-temperature threshold, *J. Appl. Phys.* **2013**, *113*, 064906–064922.
[12] C. M. Tarver, J. O. Hallquist, L. M. Erickson, Modeling short pulse duration shock initiation of solid explosives, in: Intern Symp on Detonation, Albuquerque, N Mex, 15 July **1985**.
[13] F. J. W. Tarver C M, Garcia F, Manganin gauge and reactive flow modeling study of the shock initiation of PBX 9501, *AIP Conf. Proc.* **2002**, *2*, 1043–1046.
[14] P. A. Urtiew, K. S. Vandersall, C. M. Tarver, F. Garcia, J. W. Forbes, Shock initiation of composition B and C-4 explosives: Experiments and modeling, *Russ. J. Phys. Chem. B* **2008**, *2*, 162–171.
[15] Y. Liu, T. Hussain, F. Huang, Z. Duan, Influence of Small Change of Porosity on Shock Initiation of an HMX/TATB/Viton Explosive and Ignition and Growth Modeling, *J. Energ. Mater.* **2016**, *34*, 246–259.
[16] C. M. Tarver, J. W. Kury, R. D. Breithaupt, Detonation waves in triaminotrinitrobenzene, *J. Appl. Phys.* **1997**, *82*, 3771–3782.
[17] C. M. Tarver, Ignition and Growth Modeling of LX-17 Hockey Puck Experiments, *Propellants Explos. Pyrotech.* **2005**, *30*, 109–117.
[18] R. Ames, Vented Chamber Calorimetry for Impact-Initiated Energetic Materials, *Proceedings of the 43rd AIAA Aerospace Sciences Meeting and Exhibit* **2005**.
[19] H. Wang, Y. Zheng, Q. Yu, Z. Liu, W. Yu, Impact-induced initiation and energy release behavior of reactive materials, *J. Appl. Phys.* **2011**, *110*, 239–H203.
[20] X. F. Zhang, A. S. Shi, J. Zhang, L. Qiao, Y. He, Z. W. Guan, Thermochemical modeling of temperature controlled shock-induced chemical reactions in multifunctional energetic structural materials under shock compression, *J. Appl. Phys.* **2012**, *111*, 2129–1156.
[21] X. F. Zhang, A. S. Shi, L. Qiao, J. Zhang, Y. G. Zhang, Z. W. Guan, Experimental study on impact-initiated characters of multifunctional energetic structural materials, *J. Appl. Phys.* **2013**, *113*, 2129–1156.
[22] X. Cai, W. Zhang, W. Xie, Y. Ni, D. Li, Y. Sun, Initiation and energy release characteristics studies on polymer bonded explosive materials under high speed impact, *Mater. Des.* **2015**, *68*, 18–23.
[23] Y. C. Xiao, Y. Sun, X. Li, Q. H. Zhang, S. W. Liu, H. Yang, Dynamic Mechanical Behavior of PBX, *Propellants Explos. Pyrotech.* **2016**, *41*, 629–636.
[24] Y. Xiao, Y. Sun, Y. Zhen, L. Guo, L. Yao, Characterization, modeling and simulation of the impact damage for polymer bonded explosives, *International Journal of Impact Engineering* **2017**, *103*, 149–158.
[25] X. Cai, Study on dynamic mechanical behavior and initiation characteristic of PBX, in: Doctor of Engineering, Harbin Institute of Technology, China, **2015**, pp. 107.
[26] I. F. Lan, S. C. Hung, C. Y. Chen, Y. M. Niu, J. H. Shiuan, An Improved Simple Method of Deducing JWL Parameters from cylinder expansion test, *Propellants Explos. Pyrotech.* **1993**, *18*, 18–24.
[27] P. C. Souers, R. Garza, H. Hornig, L. Lauderbach, C. Owens, P. Vitello, Metal Angle Correction in the Cylinder Test, *Propellants Explos. Pyrotech.* **2010**, *36*, 9–15.
[28] J. P. Lu, I. J. Lochert, M. A. Daniel, M. D. Franson, Shock Sensitivity Studies for PBXN-109, *Propellants Explos. Pyrotech.* **2016**, *41*, 562–571.
[29] L. Seaman, Lagrangian analysis for multiple stress or velocity gages in attenuating waves, *J. Appl. Phys.* **1974**, *45*, 4303–4314.

Received: April 3, 2018
Published online: July 24, 2018

